Performance of Generalized Spatial Modulation MIMO Over Measured 60 GHz Indoor Channels

Peng Liu, Jiri Blumenstein, Nemanja Stefan Perović, Marco Di Renzo,

Andreas Springer

Performance of Generalized Spatial Modulation MIMO over Measured 60 GHz Indoor Channels

Peng Liu, *Member, IEEE,* Jiri Blumenstein, *Member, IEEE,* Nemanja Stefan Perović, *Student Member, IEEE,* Marco Di Renzo, *Senior Member, IEEE,* and Andreas Springer, *Member, IEEE*

Abstract—In this paper, we study the capacity and symbol error probability (SEP) of generalized spatial modulation (GSM) multiple-input multiple-output (MIMO) using measured channels that are obtained by channel sounding in an indoor office environment at 60 GHz. Spatial modulation (SM) and GSM are emerging low-complexity MIMO schemes that have been extensively researched for low-GHz (below 6 GHz) communications. Recently, they have been considered and shown to be promising also for millimeter-wave (mmWave) communications. In the simplest possible case, they require only one RF chain both at the transmitter (TX) and receiver (RX), and thus are especially attractive for mmWave communications in which the number of RF chains needs to be as low as possible. Despite of some early works on the theoretical analysis of SM/GSM for mmWave communications, there have been no investigations using real-world channel data. We focus on the office line-of-sight (LOS) scenario and investigate three problems: 1) the performance of GSM using the extracted LOS component of measured channels, 2) the impact of non-LOS (NLOS) components on the performance of GSM, and 3) possible simple modulation and reception algorithms for GSM that rely only on the LOS component of the channel. The results being reported in this paper not only validate the main claims of previous studies based on ideal pure LOS channels but also lead to novel findings. One major conclusion is that NLOS components are harmful to the SEP of GSM and should be avoided. As another important outcome, our results strongly motivate the use of precoding in GSM systems to simultaneously improve the channel capacity and reduce the physical size of MIMO arrays (thus eliminating one major issue of LOS GSM).

Index Terms—Channel sounding, generalized spatial modulation (GSM), indoor, line-of-sight (LOS), multiple-input multiple-output (MIMO), millimeter-wave (mmWave), 60 GHz.

Peng Liu is with NXP Semiconductors Austria GmbH in Gratkorn (e-mail: peng.liu_6@nxp.com). Nemanja Stefan Perović, and Andreas Springer are with the Institute for Communications Engineering and RF-Systems (NTHFS), Johannes Kepler University (JKU), Linz, Austria. (e-mail: {nemanja_stefan.perovic, andreas.springer}@jku.at). The work of Peng Liu and Andreas Springer was in part supported by the Austrian COMET-K2 programme of the Linz Center of Mechatronics (LCM), which was funded by the Austrian federal government and the federal state of Upper Austria.

Jiri Blumenstein is with the Department of Radioeletronics, Brno University of Technology (BUT), Brno, Czech Republic. (e-mail: blumenstein@feec.vutbr.cz). His work was supported by the Czech Science Foundation project No. 17-27068S Mobile channel analysis and modelling in millimeter wave band and was performed in laboratories supported by the SIX project, No. CZ.1.05/2.1.00/03.0072, the operational program Research and Development for Innovation.

Marco Di Renzo is with the Laboratoire des Signaux et Systèmes, CNRS, CentraleSupélec, Univ Paris Sud, Université Paris-Saclay, 3 rue Joliot Curie, Plateau du Moulon, 91192, Gif-sur-Yvette, France. (e-mail: marco.direnzo@l2s.centralesupelec.fr). His work is partially supported by the European Commission (EC) through the H2020-ETN-5G wireless research project (grant 641985) and by the Agence Nationale de la Recherche Scientifique (ANR) through the Spatial Modulation research project (Société de l'Information et de la Communication – Action Plan 2015).
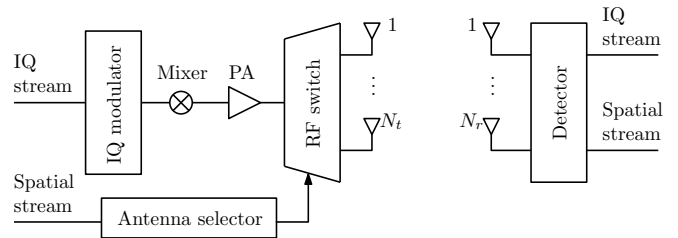
Fig. 1. Conceptual architecture for SM/GSM MIMO.

I. Introduction

SPATIAL modulation (SM) and generalized spatial modulation (GSM) are emerging low-complexity multiple-input multiple-output (MIMO) schemes for wireless communications [1]. The operating principle of SM/GSM MIMO systems [2]–[5] is radically different from that of conventional spatial multiplexing (SMX) MIMO systems, e.g., D-BLAST (Diagonal-Bell Laboratories Layered Space-Time) [6] and V-BLAST (Vertical BLAST) [7]. In SMX MIMO, the SMX gain is achieved by simultaneous transmission of multiple in-phase and quadrature (IQ) streams at the same frequency. Typically, the same number of transmitter (TX) chains (from baseband to RF) as the number of data streams are needed in SMX MIMO thus introducing significant hardware and data processing complexities. However, in SM/GSM MIMO (see Fig. 1), data streams are transmitted not only in the conventional IQ domain but also in a so-called spatial domain. SM was originally proposed to activate only a single TX antenna and transmit a single stream in the IQ domain, but was later generalized to GSM which supports multiple antenna activation and even multiple IQ stream transmission [8]–[10]. In this paper, for the sake of practical relevance to millimeter-wave (mmWave) communications, we consider the case of GSM with only a single IQ stream. The spatial domain transmission is achieved by selecting a sub-group of TX antennas for transmission of the IQ stream and modulating the spatial stream in the antenna indicies. Compared to SMX, SM/GSM can not only reduce hardware and signal processing complexities [1], but also show significantly improved TX energy efficiency [11], [12].

Extensive research has been conducted on SM/GSM [1]. However, almost all papers are concerned with SM/GSM at low-GHz (below 6 GHz) frequencies. Some early mmWave SM/GSM papers are [13]–[17], which are all concerned with the line-of-sight (LOS) scenario. A major difference between

indoor LOS mmWave SM/GSM and low-GHz SM/GSM lies in the different propagation characteristics. At mmWave frequencies, e.g., 60 GHz, the practical indoor operation range is likely to be limited by penetration loss and therefore mostly confined to a single room [14] and the indoor channel is dominated by the LOS path (if not blocked). The non-LOS (NLOS) paths, which typically suffer from 10 dB loss per reflection and additional path loss due to larger path lengths as compared to the LOS path [18], have only minor contribution to the received power. The LOS component is deterministic and determined by the relative geometries of the antennas, and this, as in LOS SMX [19], [20], gives us opportunities to optimize the performance of SM/GSM in LOS [13], [14]. In the literature and also in this paper, LOS MIMO (SMX/SM/GSM) means a MIMO communication system that is optimized based on the pure LOS component of the channel. More specifically, optimization of the symbol error probability (SEP) and channel capacity of LOS MIMO relies on proper separation of the TX and receiver (RX) antennas (by an amount that is in general much larger than half wavelength). At low-GHz frequencies, in contrast, the channels are usually rich-scattered and exhibit fading and low-coupling characteristics. Excess separation of the antennas at low-GHz is generally not necessary. Antenna separations down to half wavelength usually can lead to sufficiently low channel correlations [21, p.151] and allow exploitation of diversity and multiplexing gains [6].

So far, the work on SM/GSM, regardless of frequency, has been mainly limited to theoretical studies. Although numerical simulation and theoretical analysis serve as important and often reliable tests of the performance of novel technologies, only practical experience can yield definitive answers to their performance in real-world [4]. The only few practical works on SM/GSM are [2]–[5], all at low-GHz frequencies. In [2], a channel measurement campaign considering a 2 GHz urban channel was carried out in the city of Bristol, United Kingdom. The average bit error probability (BEP) of SM was evaluated over the measured Rayleigh fading channel. In [3], a 2×2 MIMO testbed was constructed for SM and SMX at 2.3 GHz carrier frequency. The experiment was carried out in an indoor office environment and the SM principle was validated for the first time in real-time. In [4], the indoor channel inside a teaching building was measured at 6 GHz. Both LOS (corridor-to-corridor) and NLOS (corridor-to-classroom) scenarios were measured. It was concluded that neither an independent and identically distributed (i.i.d.) nor a spatially correlated Rayleigh fading channel model, which were commonly used in theoretical works, were able to predict the behavior of SM in practical (indoor) environments. It was also concluded that owing to the higher de-correlation among antennas, the SM system performs better under NLOS scenarios than LOS scenarios. In [5], a testbed was constructed for communication using GSM with a variable number of activated TX antennas (a.k.a. VGSM) at 2.4 and 5 GHz. The experiment was carried out in an office environment and the concept of GSM was validated. These practical works proved that SM/GSM is a viable technology. But, it was also shown that the performance of SM/GSM cannot always be predicted accurately. This is because theoretical channel models are

usually too simplistic and may not capture enough details of the real-world environment.

In this paper, we study the performance of GSM that has a fixed number of activated TX antennas (a.k.a. FGSM) over measured 60 GHz (multipath) indoor channels[1]. The channel measurement was carried out in an office environment at Brno University of Technology, Czech Republic. This is the first time that SM/GSM is studied using real-world mmWave channels. GSM has been studied for application to 60 GHz indoor communications in [14], [15]. The study, however, is of theoretical nature and accounts only for the LOS component of the channel. However, practical channels may not necessarily be the same as those used for ideal pure LOS optimization. For example, NLOS paths may not be so negligible or, because of the hardware components used, the LOS paths may have different characteristics than those used in typical (theoretical) models that are used for optimizing the MIMO performance. Validation of the sensitivity or vulnerability of the optimized system to practical channels, which is the main goal of this paper, is therefore a necessary step before any real implementations. Against this background, the novel contributions of this paper are as follows:

1) We performed 60 GHz channel sounding in an indoor office environment and measured 132 channel impulse responses (CIRs). The measurement was focused on scenarios with LOS (as opposed to LOS blockage), which is the most favorable case for mmWave MIMO communications[2]. A major difference of this paper, as compared to the low-GHz indoor SM/GSM works [3]–[5], lies in the fact that GSM is optimized based on the LOS component of the channel thus making the findings provided in Section IV and Section V novel and unique.

2) We study the channel capacity of GSM using measured channels and compare it with previous theoretical results of [14] that were obtained with ideal pure LOS channels. Simulation results with the LOS component of measured channels show good agreement with the results of [14]. Further simulated results show that the NLOS components of the measured channels tend to improve the GSM capacity only when the MIMO antennas are not properly separated.

3) We study the SEP of GSM using measured channels and compare it with previous theoretical results of [14] that were obtained with ideal pure LOS channels. Simulation results with the LOS component of the measured channel show good agreement with the results of [14]. However, the measured NLOS components, though 10 dB weaker than the LOS component, show a strong disruptive effect on the SEP of GSM when practical TX and RX are

---

[1]We investigated VGSM [15] as well and found that the major claims of this paper generally also apply to VGSM.

[2]This statement is opposite to that for low-GHz MIMO, in which common belief is that NLOS and rich scattering are beneficial. For low-GHz MIMO, a rich scattering environment helps to achieve low channel correlation and a high rank channel matrix, thus facilitating simultaneous transmission of multiple data streams. At mmWave frequencies, owing to high reflection and penetration losses, the LOS component is dominant in the indoor MIMO channel. SM/GSM [13], [14], [16] and SMX [19], [20] MIMO schemes have been optimized to rely on LOS rather than NLOS propagation.

used. With the considered TX and RX schemes, this leads to the recommendation to avoid the reflected paths and exploit only the LOS paths for communication. This finding, of course, depends on the considered TX and RX schemes. Further details are provided in Section V.

4) As compared to ideal deterministic pure LOS channels, the randomness introduced by hardware nonidealities, close reflections (the NLOS components that actually merge into the LOS component due to negligible time dispersion), and more importantly precoding are found to be able to simultaneously improve the GSM capacity and reduce the physical size of MIMO arrays. This finding is a necessary supplement to the SEP optimization of [14] and capacity optimization of [15].

The rest of the paper is organized as follows. In Section II, we introduce the channel and system models, and the principle of LOS GSM. In Section III, we give details about the channel measurement, including the description of the channel sounder setup, the measurement environment and the post-processing of the measured data. In Section IV, we evaluate and analyze the capacity of GSM over the measured channels. In Section V, we evaluate and analyze the SEP of GSM over the measured channels. Finally, Section VI concludes the paper.

II. PRELIMINARIES

A. Channel Model

As shown in Fig. 2, we consider an $N_t \times N_r$ LOS MIMO system that consists of two arbitrarily placed uniform linear arrays (ULAs), where N_t and N_r are the numbers of TX and RX antennas, respectively. The antenna separations in the TX and RX ULAs are s_t and s_r, respectively, and the TX-RX distance is D, which is measured between the center points of the TX and RX ULAs. Geometrically, each ULA has two degrees of freedom, namely the azimuth angle φ and the tilt angle β (or equivalently the elevation angle $\theta = \pi/2 - \beta$). Since we are only interested in their relative geometric relations, only three angles are used — the tilt angles β_t and β_r at the TX and RX, respectively, and the azimuth angle φ_r at the RX. We limit β_t and β_r to $[0, \pi/2]$ yet still being able to cover all cases. The broadsides of the TX and RX arrays are assumed to face each other (but not necessarily parallel to each other) and the main lobes of the antennas of one array are oriented towards the other array such that LOS paths can be established between all pairs of TX and RX antennas. Otherwise, there are no further requirements on the radiation patterns of the array antennas.

For SM/GSM to operate in mmWave indoor environments, antennas with moderate gains of a few dBi are typically necessary [14]. This suggests the use of directional antennas. Motivated by this, in the channel measurement we use open-ended waveguides with a moderate gain of about 5 dBi as directional antennas (see Fig. 3). In this paper, we are interested in the performance of GSM achieved with the communication channel that includes the antennas. The antenna gain pattern, which is naturally included in the measured channel responses, is kept as it is (rather than de-embedded or deconvoluted). Due to the directivity of the antennas, the
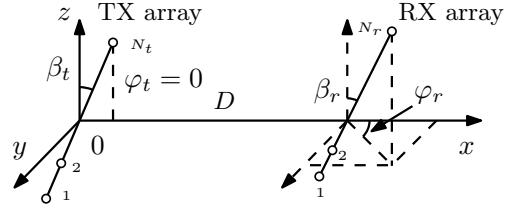

Fig. 2. LOS MIMO using arbitrarily placed ULAs. The coordinate system is chosen such that the center of the TX ULA locates at the origin and the center of the RX ULA lies on the x-axis. Furthermore, the TX ULA lies in the xz-plane, i.e., $\varphi_t = 0$.

number of propagation paths is reduced as compared to the case of using omni-directional antennas.

The impulse response of the indoor MIMO channel is commonly described as [16], [18]–[20]

$$\mathbf{H}(\tau) = \mathbf{H}_{\text{LOS}}(\tau) + \mathbf{H}_{\text{NLOS}}(\tau), \tag{1}$$

where $\mathbf{H}_{\text{LOS}}$ and $\mathbf{H}_{\text{NLOS}}$ are $N_r \times N_t$ matrices respectively representing the LOS and NLOS components of the channel, and τ is the time in the delay domain. The LOS component is assumed to be always present. The j, i-th element of the channel matrix $\mathbf{H}$, which represents the sub-channel between the i-th TX antenna and the j-th RX antenna, is given by [18], [20]

$$
\begin{aligned}
h_{ji}(\tau) = \sum_{k=1}^{K} & G_{\text{TX}}\left(\varphi_{\text{TX}}^{(k)}, \theta_{\text{TX}}^{(k)}\right) G_{\text{RX}}\left(\varphi_{\text{RX}}^{(k)}, \theta_{\text{RX}}^{(k)}\right) \\
& \times \alpha_{ji}^{(k)} \delta(\tau - \tau_{ji}^{(k)}),
\end{aligned}
\tag{2}
$$

where K is the number of paths, $\varphi_{\text{TX}}^{(k)}$, $\theta_{\text{TX}}^{(k)}$, $\varphi_{\text{RX}}^{(k)}$ and $\theta_{\text{RX}}^{(k)}$ are, respectively, the TX azimuth, TX elevation, RX azimuth and RX elevation angles of the k-th path, G_{TX} and G_{RX} are, respectively, the TX and RX gains in the direction of the path, $\alpha_{ji}^{(k)}$ is the amplitude of the path, $\delta(\cdot)$ is the Dirac delta function, and $\tau_{ji}^{(k)}$ is the propagation delay of the path. The path delay is related to the path length $d_{ji}^{(k)}$ by the speed of light c as $\tau_{ji}^{(k)} = d_{ji}^{(k)}/c$. For each sub-channel h_{ji}, there is a single LOS path which is contained in $\mathbf{H}_{\text{LOS}}$. The other $K - 1$ paths are NLOS and are contained in $\mathbf{H}_{\text{NLOS}}$. As for the LOS paths, the α in (2) is given according to the Friis's transmission equation [22] by

$$\alpha_{ji}^{(1)} = \frac{\lambda}{4\pi d_{ji}^{(1)}}, \tag{3}$$

where λ is the wavelength of the center frequency, and $d_{ji}^{(1)}$ is the length of the LOS path between the i-th TX antenna and the j-th RX antenna. As for the NLOS paths, the α in (2) includes, in addition to the path loss, also the reflection coefficient(s) [20], and is given by

$$\alpha_{ji}^{(k)} = \frac{\lambda}{4\pi d_{ji}^{(k)}} \prod_{r=1}^{R} \Gamma_r^{(k)}, \quad k = 2, 3, \ldots, K \tag{4}$$

where $d_{ji}^{(k)}$ is the length of the k-th (NLOS) path between the i-th TX antenna and the j-th RX antenna, $\Gamma_r^{(r)}$ is the reflection

coefficient of the r-th reflection of the k-th (NLOS) path that is determined by the material of the surface [23], and R is the number of reflections of the path.

The channel model above provides us with the necessary information for understanding the behavior of the channel. It is worth mentioning, however, that the objective of this paper is to quantify the system performance via measured channels, rather than extracting the above mentioned channel parameters from the measurements. Therefore, the latter issue is left to future analysis.

B. Principle of GSM

In this subsection, we introduce the basic principle of LOS GSM. For ease of presentation, we consider only the (dominant) LOS component of the channel. The impact of NLOS components on the performance of LOS GSM will be considered later in the capacity and SEP analyses in Section IV and Section V.

Since only the LOS component is considered, it is more convenient to use an equivalent form to the $\mathbf{H}_{\text{LOS}}$ modeled in Section II-A, in which the j, i-th element is alternatively given by

$$\underline{h}_{ji} = \frac{\lambda}{4\pi \underline{d}_{ji}} \exp(-\mathbb{j} k \underline{d}_{ji}), \tag{5}$$

where $k = 2\pi/\lambda$ is the wave number, and $\mathbb{j}$ is the imaginary unit. The received signal vector $\mathbf{y} \in \mathbb{C}^{N_r \times 1}$ is given by

$$\mathbf{y} = \mathbf{H}_{\text{LOS}} \underbrace{q_m \mathbf{e}_i}_{\triangleq \mathbf{x} \in \mathbb{S}} + \mathbf{n} = q_m \sum_{k \in \mathcal{I}_i} \underline{\mathbf{h}}_k + \mathbf{n}, \tag{6}$$

where

q_m is an IQ (e.g., M-QAM or M-PSK) symbol, and $m = 1, \ldots, M$ is the IQ symbol index;

$\mathbf{e}_i$ is a spatial symbol which is an $N_t \times 1$ vector containing N_u ones (representing the activated TX antennas) and $N_t - N_u$ zeros (representing the inactivated TX antennas), and $i = 1, \ldots, \binom{N_t}{N_u}$ is the spatial symbol index;

$\mathbb{S}$ $\triangleq \{q_m \mathbf{e}_i \mid i = 1, \ldots, \binom{N_t}{N_u} \text{ and } m = 1, \ldots, M\}$ is the GSM modulation alphabet;

$\mathbf{x}$ $\in \mathbb{S}$ is a transmitted GSM symbol;

$\mathcal{I}_i$ $\triangleq \{k \mid k \in \{1, \ldots, N_t\} \text{ and } \mathbf{e}_i(k) = 1\}$ is the set of indices of the activated TX antennas corresponding to the i-th spatial symbol;

$\underline{\mathbf{h}}_k$ $\triangleq [\underline{h}_{1k}, \underline{h}_{2k}, \ldots, \underline{h}_{N_r k}]^T$ is the k-th column of $\mathbf{H}_{\text{LOS}}$;

$\mathbf{n}$ $\in \mathbb{C}^{N_r \times 1}$ is the i.i.d. additive white Gaussian noise (AWGN) vector which has a covariance matrix $N_0 \mathbf{I}_{N_r}$ ($\mathbf{I}_{N_r}$ is the $N_r \times N_r$ identity matrix).

Due to transmission of only a single IQ stream and TX antenna switching, the received signal vector at the RX contains a combination of N_u columns of the channel matrix which are multiplied by the same IQ symbol q_m. This is different from the SMX, in which the received signal typically contains a combination of multiple columns of the channel matrix which are multiplied by different IQ symbols.

In GSM, there are $\binom{N_t}{N_u}$ activation patterns of the TX antennas thus achieving a spatial data rate of $\log_2 \binom{N_t}{N_u}$ bpcu
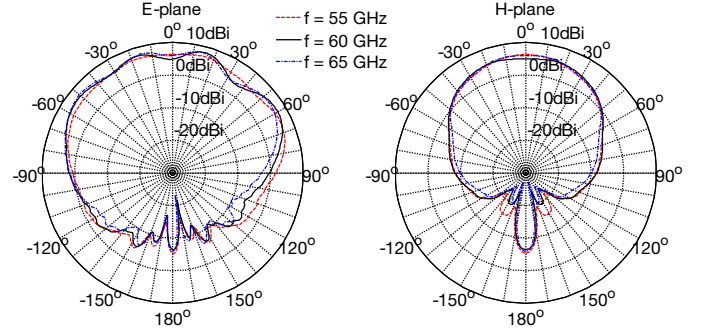

Fig. 3. Measured gain pattern of the open-ended waveguide antennas in the E- and H-planes.

and a total data rate of $\log_2 \binom{N_t}{N_u} + \log_2 M$ bpcu. The maximum rate is achieved when $N_u = \lfloor N_t/2 \rfloor$. This is due to the fact that for a given N_t, $\binom{N_t}{N_u}$ is a symmetric concave function of N_u that is centered around $N_t/2$. In contrast, single-antenna activation SM achieves a spatial rate of $\log_2 N_t$ bpcu and a total rate of $\log_2 N_t + \log_2 M$ bpcu.

C. Optimal Detection

Under the assumption of a pure LOS MIMO channel, the optimal detector for GSM that is based on the maximum likelihood (ML) principle is well-known to be given by [24]

$$\begin{aligned} (\hat{i}, \hat{m}) &= \arg\max_{i,m} p_{\mathbf{y}} \left(\mathbf{y} \mid s_{i,m}, \mathbf{H}_{\text{LOS}} \right) \\ &= \arg\min_{i,m} \|\mathbf{y} - \mathbf{H}_{\text{LOS}} q_m \mathbf{e}_i\|, \end{aligned} \tag{7}$$

where $p_{\mathbf{y}}(\cdot)$ denotes the probability density function (PDF) of $\mathbf{y}$, and $\|\cdot\|$ denotes the Euclidean distance.

D. Optimized Channel Conditions

The deterministic nature of the LOS component of the channel gives us the opportunity of optimizing the performance of GSM. Optimization of the capacity and SEP for GSM based on the LOS component $\mathbf{H}_{\text{LOS}}$ is found in [14], [15]. The relevant findings are as follows.

To minimize the SEP of GSM, $\mathbf{H}_{\text{LOS}}$ has to be column-orthogonal, which in turn requires the TX and RX antennas to be properly separated. The minimum antenna separation product (ASP) is given by [14]

$$s_t s_r \approx D\lambda\zeta/N_r, \tag{8}$$

where $\zeta \triangleq 1/(\cos\beta_t \cos\beta_r)$ is the so-called tilt factor which measures the degree of tilt of the ULAs. In addition, we need $N_r \geq N_t \geq 2$, where $N_r \geq N_t$ is necessary in order to have N_t orthogonal channel columns and $N_t = 2$ is the minimum number of TX antennas needed for SM/GSM to operate. Perfect orthogonality is lost if the actual ASP differs from the optimal value. To measure this, we use an ASP deviation factor η which was previously defined in [25] as

$$\eta = \frac{\text{Minimum ASP for orthogonality}}{\text{Actual ASP}} = \frac{D\lambda\zeta/N_r}{s_t s_r}, \tag{9}$$

where the minimum ASP for orthogonality is given in (8). Note that the term $s_t s_r$ in the denominator of (9) denotes the actual

ASP and should not be confused with the optimal ASP (to achieve channel orthogonality) given in (8). If the actual ASP is larger than the optimal ASP, we have $\eta < 1$; if the actual ASP is smaller than the optimal ASP, we have $\eta > 1$. In what follows, we use η as an (inverted) normalized ASP.

The orthogonality condition (8) usually means excess antenna separations and array lengths. In practice it is very likely that the antennas are under-separated, i.e., $\eta > 1$. Therefore, in this paper we restrict the study to $\eta \geq 1$.

Actually, to maximize the capacity of LOS GSM, $\eta = 1$ tends only to be needed at a moderate signal-to-noise ratio (SNR). At low SNR, beamforming gain is more important and the optimal η tends to be infinity, i.e., the intra-array antenna separations of the TX and RX ULAs should be as small as possible. At high SNR, the optimal η tends to increase with increasing SNR. For example, for a 6×6 ($N_t \times N_r$) system, the optimal η increases from 1 to 6 when the SNR increases from 5 to 30 dB [15, Fig. 7].

III. Channel Measurements

A. Measurement Environment and Scenarios

As far as LOS MIMO communications is concerned, it is especially true that the system performance is primarily determined by the installation of TX and RX antennas and the surrounding environment. The channel sounding campaign was performed in a laboratory/office environment at the Brno University of Technology (see Fig. 4), and the measurement captures two typical use cases of LOS GSM, which we denote as measurement Scenario I and measurement Scenario II. The difference between the two scenarios lies mainly in the measurement site geometry (medium-size laboratory vs. small-size laboratory) and the fact that in Scenario I many reflective surfaces were covered by absorbers.

1) Scenario I: Scenario I accounts for a medium-size laboratory ($15\,\mathrm{m} \times 6\,\mathrm{m} \times 2.8\,\mathrm{m}$) that is shown in Fig. 4(a). Absorbers were used to suppress reflections from the floor and metallic table legs. The purpose of using absorbers is two-fold: 1) to make the measured LOS component as much closer to ideal propagation conditions as possible — free of close reflections, i.e., NLOS components that actually merge into the LOS component due to negligible time dispersion — but still allowing reflections from the ceiling and walls, and 2) to better highlight the differences with Scenario II, where no absorbers are used. The TX-RX distance is $3\,\mathrm{m}$ and the height of the TX and RX antennas above the ground is $1.2\,\mathrm{m}$.

Both the TX and RX antennas are placed on xy-tables with a sub-millimeter shifting step. As indicated in Fig. 4(a) with red lines, with proper alignment of the TX and RX xy-tables (which, according to Fig. 2, means azimuth angles $\phi_t = \phi_r = 0$, tilt angles $\beta_t = \beta_r = \pi/2$, and $\eta = 1$), virtual TX and RX ULAs can be emulated using a single pair of antennas. In this scenario, four sets of data were measured corresponding to a 4×4 MIMO system with $\eta = 1, 2, 4$ and a 6×6 MIMO system with $\eta = 1$.

2) Scenario II: Scenario II accounts for a smaller-size laboratory ($6\,\mathrm{m} \times 6\,\mathrm{m} \times 2.8\,\mathrm{m}$) (see Fig. 4(b)). In this scenario, the TX-RX distance is reduced to $2.5\,\mathrm{m}$. The TX-RX link is
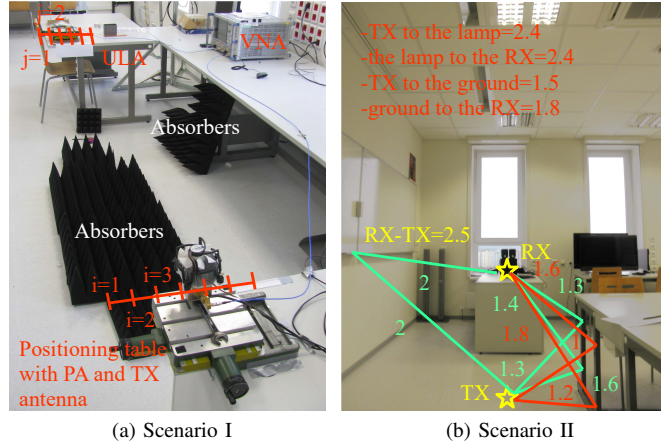

(a) Scenario I   (b) Scenario II

Fig. 4. The measurement site. All dimensions in (b) are in meters.

close to a wall on the left side and no absorbers are used to shield the ground and metallic table legs. As a result, a richer scattering environment is created. The antenna hight, tilt angles and measurement procedure are, on the other hand, the same as those of Scenario I. Three sets of data were measured corresponding to a 4×4 MIMO system with $\eta = 1, 2, 4$ in this scenario.

Despite the use of absorbers, Scenario I can be considered to be a representative example of the channel conditions that are typically encountered in the STA-AP sub-scenario of IEEE 802.11 WLAN [18], where the AP (access point) is installed on the ceiling and the STA (station, or communication device) is placed on a table in the same room. In this regard, Scenario II can be viewed as an emulation of the STA-STA (device to device) sub-scenario of WLAN. In total, we obtained 7 virtual MIMO realizations and 132 CIRs for the two scenarios.

B. 55–65 GHz Channel Sounder

The channel sounder is composed of a vector network analyzer (VNA) and a pair of TX and RX antennas. The MIMO channel is measured by changing the positions of the TX and RX antennas on xy-tables. The channel sounder operates based on the frequency domain measurement principle illustrated in [26], [27] (as opposed to the time-domain principle presented for the mmWave band in [28]). In the frequency-domain method, a narrow-band continuous wave signal is used to sound the channel and the signal is swept from 55 to 65 GHz with a step size of 10 MHz.

The R&S ZVA67 four-port VNA is utilized to measure the transmission coefficient between TX and RX antennas. Perfect synchronization between the TX and RX is achieved because of the use of a VNA. The system dynamic range of the measurement setup is extended utilizing a broadband power amplifier (QuinStar QPW-50662330), which has a measured gain of 35 dB in the band of interest, on the TX side. Similar to [29], we use two WR15 open waveguides, which have the radiation pattern as shown in Fig. 3, as the TX and RX antennas. Phase-stable coaxial cables are used in order to avoid the degradation of the measured phase accuracy due to the

movements of the TX and RX antennas. A VNA output power of 5 dBm and IF bandwidth of 100 Hz are used. The system's dynamic range of this channel sounder is approximately 50 dB.

Before channel sounding, a full 4-port calibration process was performed including the power amplifier (PA) with WR15 output. Therefore, as we utilize the open-ended waveguide as both the RX and TX antenna, the antenna gains are included in the calibration process.

C. Data Acquisition and Post Processing

As the measurement environment has no moving objects, the measured radio channel is considered to be time invariant. The measured frequency domain channel transfer function (CTF) is given by

$$\tilde{h}_{ji}(g) = s^{21}_{ji}(g), \qquad (10)$$

where g is any of the measurement frequencies, i, j are, respectively, the indices of the elements of the virtual TX and RX ULAs, and s^{21} is the S-parameter representing the transmission from the feed of the TX antenna to the output of the RX antenna. By invserse Fourier transform (IFT), we convert the CTF into the CIR as

$$h_{ji}(n) = \sum_{g=0}^{L-1} \tilde{h}_{ji}(g) \exp\left(\mathbb{j}\frac{2\pi g n}{N}\right), \qquad (11)$$

where $h_{ji}(n)$ is the measured discrete version of the ji-th element of the multipath channel $\mathbf{H}$ given in (1).

D. Validation of the Measured Data

In short range indoor LOS communications, the channel usually contains a long diffused tail because of reflections [30]. In our experiments, we consider a setup where the first few Fresnel zones are free of obstacles, but there are a sufficient number of reflections outside them. As an example, the measured CIRs for a 4×4 MIMO system with $\eta = 4$ for the two scenarios described in Section III-A are plotted in Fig. 5. We see that the measured LOS component is located at the correct positions for both scenarios — at $D = 3\,\mathrm{m}$ for Scenario I and at $D = 2.5\,\mathrm{m}$ for Scenario II. The reason of the presence of the NLOS clusters are discussed in the sub-figures themselves. By comparing Fig. 5 (a) and (b), it is evident that the reflections from the metallic table legs and the ground are effectively suppressed in Scenario I due to the use of absorbers. It is apparent, in addition, that Scenario II represents a richer scattering environment as compared to Scenario I.

As an example, the LOS component of the measured 4×4 MIMO with $\eta = 1$ is plotted in Fig. 6 for the two scenarios. At 60 GHz, the free space path loss (FSPL) for $D = 3\,\mathrm{m}$ excluding the TX and RX antenna gains of 5 dBi is 77.6 dB. Taking into account possibly $2 \times 1\,\mathrm{dB}$ cable and connector losses at the TX and RX, the average measured path loss including the antenna gains should be around 69.6 dB. This is confirmed by direct inspection of Fig. 6(a). It can be similarly verified that the measured mean path loss in Fig. 6(b) is reasonable as well. However, in the sub-figures, we can observe some variations around the expected (theoretical) means, i.e., 0.42 dB and 0.33 dB in Fig. 6 (a) and (b), respectively. These variations

are not shown in the corresponding curves for ideal pure LOS channels. We attribute these variations to hardware nonidealities and disturbance from close reflections.

IV. CAPACITY ANALYSIS

In this section, we present simulation results on the capacity of GSM over measured channels. More specifically, we study the performance of the measured LOS component and the impact of the NLOS components of the measured multipath channels on the capacity of GSM. Three case studies are analyzed: 1) the capacity is evaluated with ideal pure LOS channels; 2) the capacity is evaluated with the LOS component extracted from the measured multipath channels; and 3) the frequency-average capacity is evaluated with the measured multipath channels. In addition, the capacity achieved by ideal pure LOS channels is used as a benchmark.

Although the measurement covers a bandwidth of 10 GHz centered at 60 GHz, both the capacity in this section and the SEP in the next section are evaluated by considering a more practical bandwidth of 1 GHz. This bandwidth is still centered around 60 GHz. This is obtained by discarding the CTF that lies outside the band of interest before converting it to the time-domain CIR (see Section III-C).

A. Capacity Evaluation

The LOS component of the measured MIMO channels is not time-dispersive, which means that the relative time delays between the LOS paths are much smaller than the symbol duration. Otherwise, the channel is time-dispersive. The capacity of GSM over non-time-dispersive channels can be evaluated by using (12) given in Appendix A-1. However, the complete measured channels as shown in Fig. 5 are time-dispersive and therefore are frequency-selective in the sense that the channel coefficients vary over frequency. Based on the same consideration as given in [15, Section III-B], the capacity of GSM over the measured channels is evaluated on a narrow band (frequency-flat) basis by using (12) and is averaged over frequency. Further details are available in Appendix A-2.

B. Simulation Results

We first concentrate on Scenario I, and the simulation results on the capacity of GSM are shown in Fig. 7. Each sub-figure corresponds to one set of the measured channel data, and the FSPL due to the TX-to-RX distance D is not counted in the SNR that is shown on the abscissa.

1) Capacity of the Measured LOS Component: As far as the orthogonal setups are concerned, i.e., 4×4 and 6×6 MIMO both with $\eta = 1$ as shown in Fig. 7(a)–(b), the LOS component of the measured channels shows identical performance as the ideal pure LOS channels. The effect of the variations in the power of the LOS paths in Fig. 6 is not visible in this case.

As far as the non-orthogonal setups are concerned, i.e., 4×4 MIMO with $\eta = 2, 4$ as shown in Fig. 7(c)–(d), the capacity of GSM using the LOS component of the measured channels does not perfectly match the curves of the ideal pure LOS channels.
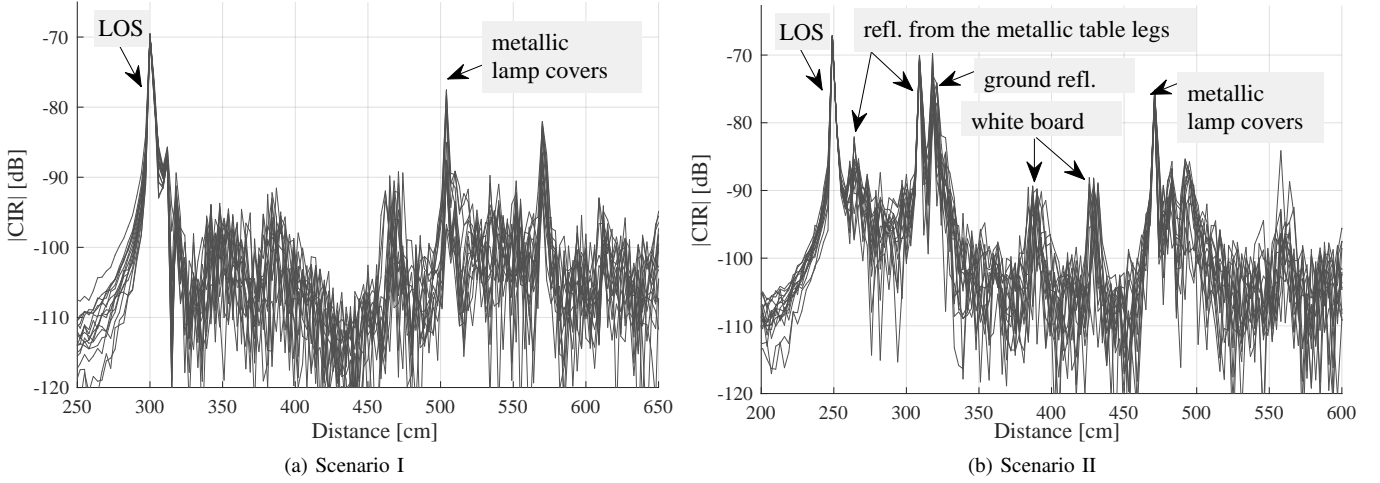
(a) Scenario I

(b) Scenario II

Fig. 5. Measured CIRs for 4×4 MIMO with $\eta = 4$. All 16 CIRs are plotted in each sub-figure.

(a) Scenario I, 4×4 MIMO with $\eta = 1$

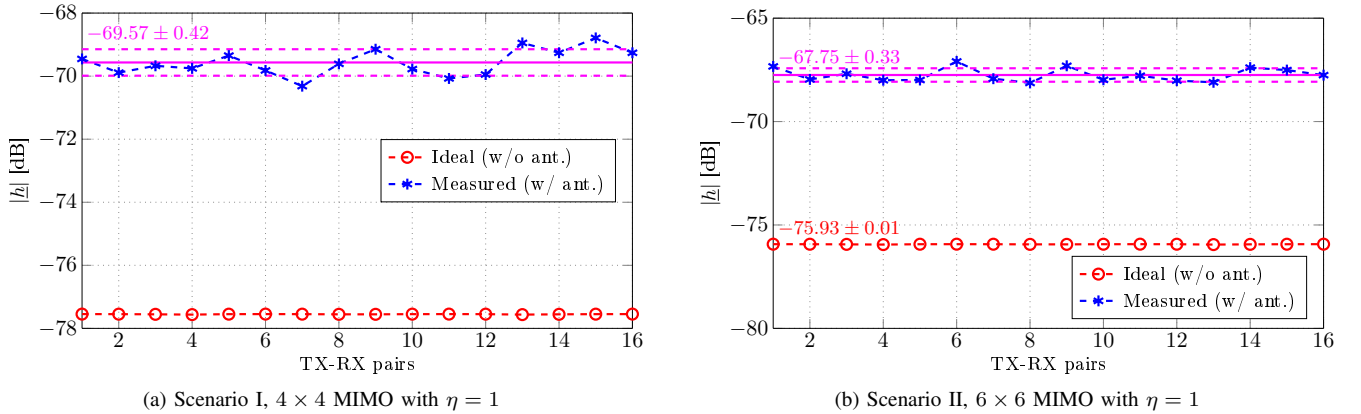
(b) Scenario II, 6×6 MIMO with $\eta = 1$

Fig. 6. Magnitudes of measured LOS paths (including TX and RX antennas) vs. the magnitudes of simulated LOS paths (excluding TX and RX antennas). The mean and standard deviation of the measured magnitudes are evaluated in dB scale and indicated with magenta lines.

Comparing Fig. 7(a), (c) and (d), all for 4×4 MIMO but with $\eta = 1$, 2 and 4 respectively, we note that, with increasing η, the capacity of GSM using the LOS component of the measured channels is increasingly worse compared to that of ideal pure LOS channels. By direct inspection of Fig. 7, we find that:

- The IQ capacity C_1 of the measured LOS component is worse than that of ideal pure LOS channels with increasing η. Actually, C_1 of the measured LOS component itself is not noticeably worsened for increasing η, but rather it does not show the increment that is shown by ideal pure LOS channels.
- The spatial capacity C_2 of the measured LOS component, however, seems to be better than that of ideal pure LOS channels with increasing η. Actually, C_2 of the measured LOS component does not seem to be improved due to increased η, but rather it does not show the deficiency that is shown by ideal pure LOS channels.

To further investigate the impact of hardware nonidealities and randomization of the channel on the GSM capacity, we performed capacity simulations by adding artificial randomness on top of deterministic ideal LOS channels. The randomness may represent the contribution from hardware imperfections,

close reflections[3] and precoding. More specifically, we are interested in the case of under-separated MIMO setups (i.e., $\eta > 1$), which means shrunk physical size of the MIMO arrays. As a result, the following findings were obtained. If the MIMO setup is under-separated (i.e., $\eta > 1$), the GSM capacity can indeed be improved by adding sufficient randomness to the channel matrix. We experimented by adding AWGN on top of deterministic LOS channel components, and found that the GSM capacity of 4×4 MIMO with $\eta = 10$ can be maximized by adding AWGN with a power of at least $-3\,\mathrm{dB}$ in relation to the average LOS path strength (see Fig. 8). For fairness of comparison, the channel matrices (with/without added randomness) are normalized such that the average strengths of the LOS paths are unitary. Taking a close look at the two sets of curves (with/without channel randomization) for $\eta = 10$ in the figure, we see that, at moderate SNR (0–20 dB), the artificial channel randomness added brings clear improvement to the spatial

---

[3]It has to be noted that along with the channel randomization effect, close reflections may have a cancellation effect. For example, table reflections can be out of phase [18] and the dominant effect may be performance degradation rather than enhancement due to cancellation.
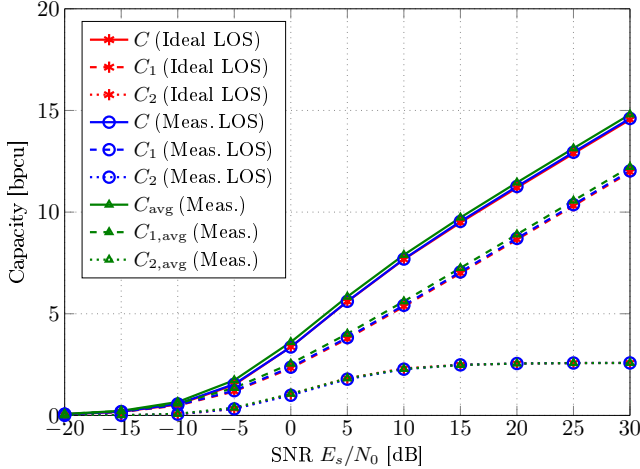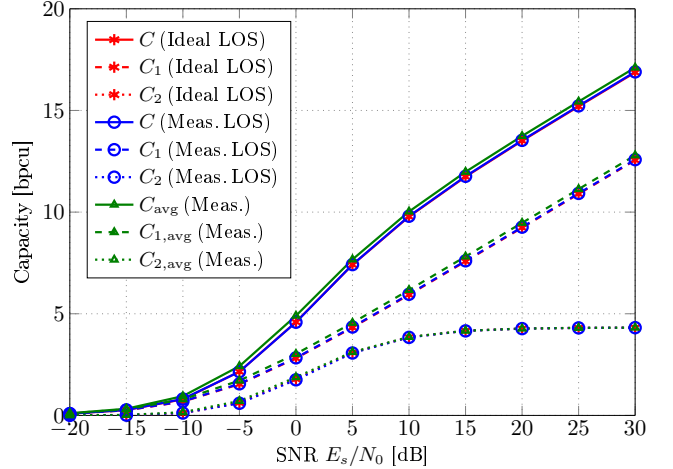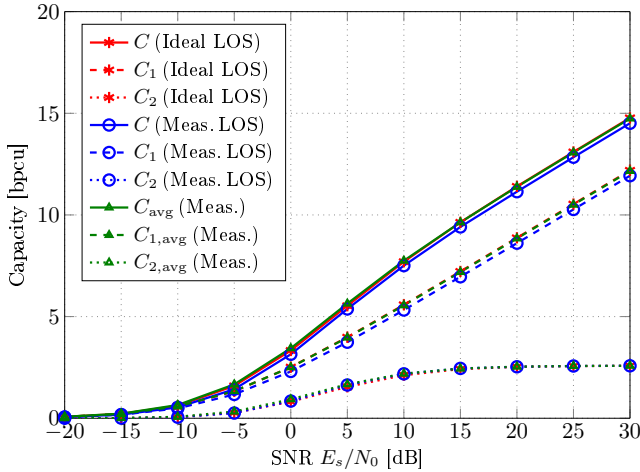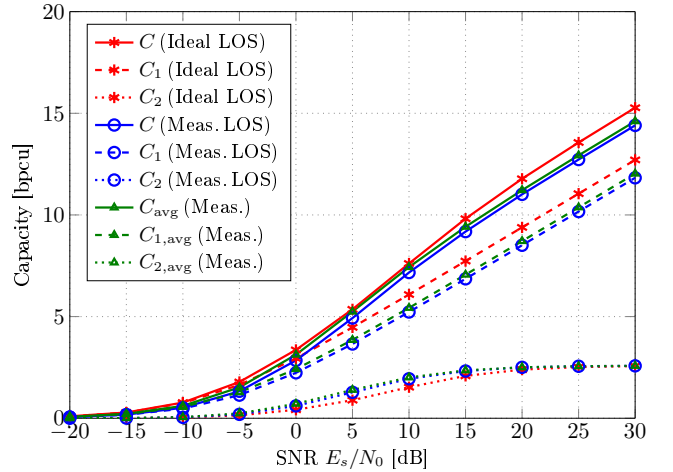
(a) Scenario I, 4×4 MIMO with $\eta = 1$

(b) Scenario I, 6×6 MIMO with $\eta = 1$

(c) Scenario I, 4×4 MIMO with $\eta = 2$

(d) Scenario I, 4×4 MIMO with $\eta = 4$

Fig. 7. Simulation results on the capacity of GSM (Scenario I). Legend: "Ideal LOS" — ideal pure LOS channels; "Meas. LOS" — LOS component extracted from measured multipath channels; "Meas." — measured multipath channels including both LOS and NLOS components.

capacity[4], while at the expense of marginal degradation in IQ capacity[5]. As a result, the total GSM capacity is improved as compared to the same setup ($\eta = 10$) but with ideal LOS paths. Moreover, we see that with the randomness added, the setup with $\eta = 10$ achieves superior total GSM capacity than the case with ideal LOS paths and $\eta = 1$[6].

---

[4]This is because the spatial capacity (C_2 in (12)) is limited by small Euclidean distances between certain pairs of the RX-side spatial symbols, which arose from the under-separation of the MIMO setup, and the randomness added increased the small Euclidean distances statistically such that the spatial symbols became less ambiguous.

[5]This is because, due to the randomness added, the average array gain for IQ domain transmission is reduced. To further elaborate, we know from the maximal ratio combining (MRC) principle that, when the noise level is equal over different branches, the optimum strategy is to have equal gains. In our system, the noise level is indeed assumed to be equal over different RX branches, thus the variations in the LOS path strength introduced by artificial randomness degrades array gain and reduces the IQ capacity.

[6]A side comment is that, as compared to the case with orthogonal MIMO setup ($\eta = 1$), higher IQ capacities are shown in the two cases with under-separated MIMO setup ($\eta = 10$). This is because there is no TX array gain in the orthogonal setup. While in the under-separated setup, certain amount of TX array gain is exhibited due to reduced antenna separations.

To sum up, the above results allow us to conclude the following:

- The capacity of GSM as predicted by ideal pure LOS channels in [14] can indeed be achieved in practice with orthogonal MIMO setups.
- As for under-separated MIMO setups (i.e., $\eta > 1$), channel randomization that may be introduced by hardware imperfections, close reflections and precoding shows the capability to simultaneously improve the GSM capacity and reduce the MIMO array size.
- The results in Fig. 8 strongly motivate us to use precoding [31], [32] with GSM. We thus gain maximized GSM capacity and, more notably, significantly shrunk physical size of the MIMO arrays.

2) Impact of Non-LOS Components on Capacity: The frequency-average capacity is evaluated at the measured frequency points and averaged over a 1-GHz bandwidth that is centered at about 60 GHz. The simulation results are presented in Fig. 7. We notice that the NLOS components of the measured channels show a marginal improvement of the IQ capacity C_1
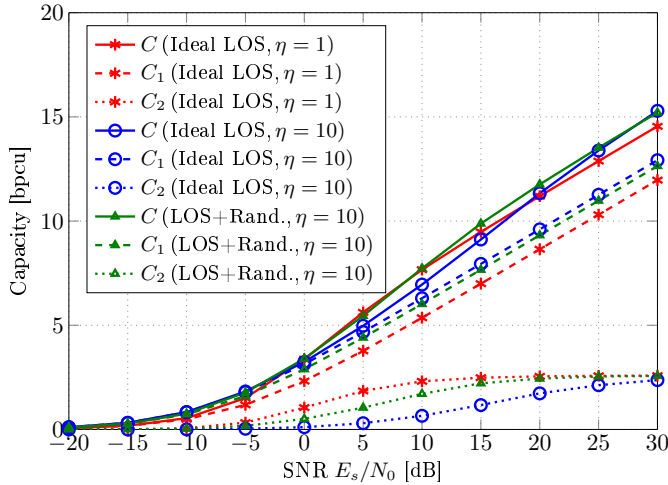
Fig. 8. Effect of channel randomization on the capacity of GSM. The MIMO size is 4×4, and "LOS+Rand." refers to that AWGN with -3 dB power in relation to the average LOS path strength is added on top of the deterministic LOS channel component. For fairness of comparison, the channel elements are all normalized to unit average power.
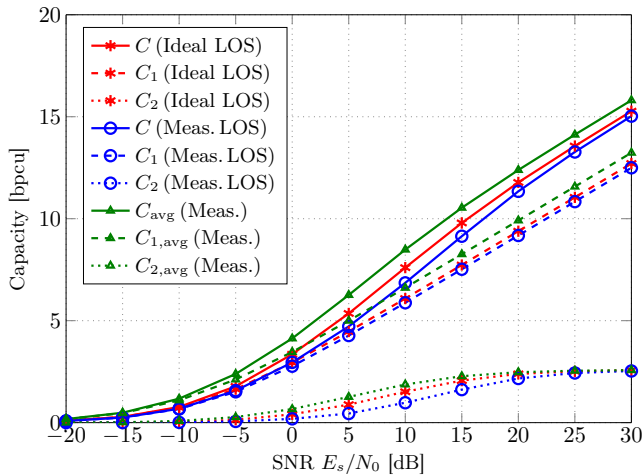

Fig. 9. Simulation results on the capacity of GSM (Scenario II, 4×4 MIMO with $\eta = 4$). The legend terms are the same as in Fig. 7.

but no improvement of the spatial capacity C_2. In summary, the NLOS components of the measured channels provide only marginal improvement on the total capacity C of GSM.

3) Impact of Richer Scattering and Close Reflections: As far as this case study is concerned, we consider Scenario II, which, in contrast to Scenario I, is characterized by richer scattering and close reflections. After performing capacity evaluations with the measured data of Scenario II and comparing it with the results of Scenario I in Fig. 7 (a), (c) and (d), we have the following findings. Due to space limitation, we show only one figure, i.e., Fig. 9, which corresponds to the case study of 4×4 MIMO with $\eta = 4$.

- In Scenario II, both the GSM capacity of the LOS component of the measured channels and the frequency-average GSM capacity of the measured multipath channels are in agreement with those predicted by using ideal pure LOS channels.

- The frequency-average GSM capacity is improved as compared to the GSM capacity of ideal LOS channels in all cases, i.e., $\eta = 1, 2, 4$ (see Fig. 9 for the case of $\eta = 4$). By contrast, there was no such improvement in Scenario I in Fig. 7.

V. SEP ANALYSIS

In this section, we study the SEP of GSM over the measured channels. More specifically, we investigate the following case studies: 1) the SEP of GSM over the LOS component of the measured channels, 2) the impact of the NLOS components of the measured multipath channels on the SEP of GSM, 3) the impact of the NLOS components on the SEP of reduced-complexity (for the sake of practicability) GSM systems, and 4) the impact of richer scattering and close reflections on the SEP of GSM. The SEP of GSM over ideal pure LOS channels is used as a benchmark.

A. Simulation Algorithms

As shown in Fig. 5, the measured channels exhibit a time dispersion time of the order of tens of nanoseconds, which causes an intersymbol interference (ISI) of the order of tens of symbols if we transmit at a symbol rate of the order of 1 GHz. To handle the ISI, we use a receiver that is based on single carrier (SC)-frequency domain equalization (FDE) (see Appendix B-2 for details). Another solution to handle the ISI issue could be to use orthogonal frequency-division multiplexing (OFDM) and apply GSM on a sub-carrier basis. However, per sub-carrier GSM makes it impossible to implement the switching at RF. Instead, baseband switching, which requires N_t full TX chains (from baseband to RF), is needed. Accordingly, baseband detection, which requires N_r full RX chains (from RF to baseband), is needed. We refer to such a system as having a full-complexity TX and RX. In such a solution, one big motivation for SM/GSM — single-RF TX (and simple detection) — is lost. Since hardware and computational complexity is a major concern at millimeter frequencies, the per-subcarrier GSM option is not studied in the present paper. The interested reader may find further details in [33]. In SC-FDE GSM, on the other hand, a simple TX based on RF switching can still be used. We refer to such a system as having a simple TX but full-complexity RX.

Despite of a simple TX, SC-FDE GSM still requires a full-complexity RX, which implies N_r full RX chains from RF to baseband. This may be acceptable in practice if N_r is a small number. In current implementations of mmWave MIMO systems, however, it may not always be practical to dedicate a separate RF chain to each available antenna [34], [35]. Motivated by these implementation constraints, we study the SEP performance of a low-complexity reception scheme which does not necessitate N_r RF chains and is based on a detection algorithm without equalization (see Appendix B-3 for details). In this proposed algorithm, the NLOS components of the channel are ignored and only the LOS component is used for detection. This scheme, besides avoiding both full TX and full RX complexities, leads to a simple RX that can be implemented based on RF phase shifters and a single IQ

down-conversion and sampling chain [14]. We refer to such a system as having full simplicity.

B. Simulation Results

Similar to the capacity analysis in Section IV, we first concentrate on Scenario I and subsequently study Scenario II and compare it with the former case study.

1) SEP over Pure LOS Channels: To study the SEP of GSM over the extracted LOS component of the measured multipath channels, the direct ML detection algorithm without FDE given in (7) is used and the simulation results are presented in Fig. 10. The findings are as follows.

We observe that the SEP of GSM over ideal LOS channels is better if $\eta = 1$ (in Fig. 10 (a) and (b)) as compared to that for $\eta > 1$ (in Fig. 10 (c) and (d)). This agrees with the prediction of [14] that the SEP of GSM in the pure LOS scenario can be minimized by making the channel orthogonal (i.e., $\eta = 1$).

If the MIMO setup is non-orthogonal (i.e., $\eta \neq 1$), on the other hand, the nonidealities — the fluctuations of the measured magnitudes as shown in Fig. 6 — in the measured LOS component can play an important role. As shown in Fig. 10 (c) and (d), if the MIMO setup is non-orthogonal but with reduced ASP, i.e., $\eta > 1$, both the SEP over ideal LOS channels and the SEP over the LOS component of the measured channels deteriorate and are worse for larger η. In this latter case, however, we notice that the SEP over the LOS component of the measured channels is much better than that over ideal pure LOS channels. This is mostly visible in Fig. 10(d), where the SEP over the measured LOS component is better than that over the corresponding ideal pure LOS channel by 5 dB at an error probability equal to 10^{-3}.

Based on this experimental study, we conclude that the simulation results agree with the prediction of [14] that the SEP of GSM in the pure LOS scenario can be minimized by making the MIMO channel orthogonal. Nonidealities in the measured LOS component, however, are likely to play an important role and greatly improve the SEP of GSM if the MIMO antennas are under-separated.

To further investigate the role played by the aforementioed nonidealities, we apply the precoding method of [31] to the set of channel data that is used in Fig. 10(d). The simulation results are plotted in Fig. 11. It is shown that pure precoding and precoding on top of the nonidealities show similar error performance which is about 6 dB improvement with respect to the ideal LOS channel at high SNR. In the example, roughly 5 dB gain is attained by the nonidealities even without precoding. On top of that, precoding has another 2 dB gain, but at the expense of extra hardware (see [31] for details of the precoding structure).

2) Multipath Channel with SC-FDE Reception: Here we study the SEP of GSM over the measured multipath channels by considering the SC-FDE reception scheme that is given in Appendix B-2. As for orthogonal MIMO setups (i.e., $\eta = 1$), Fig. 10 (a) and (b) show that the SEP of GSM over measured multipath channels with FDE reception is slightly worse (within 2 dB in terms of SNR) than that over the extracted LOS component of the measured multipath channels. As for MIMO setups with reduced ASP (i.e., $\eta > 1$), on the other hand, Fig. 10 (c) and (d) show that the SEP over measured multipath channels with SC-FDE reception is significantly worse (e.g., 10 dB in SNR at an SEP level equal to 10^{-3}) than that of the extracted LOS component of the measured multipath channels.

These findings lead to the conclusion that, as far as the SC-FDE reception scheme is concerned, the NLOS components are harmful to the error performance of GSM if the LOS component is present (i.e., not blocked). From the SEP perspective, as a result, the NLOS components deteriorate the achievable performance of GSM. From the implementation perspective, despite of a simple TX, a full-complexity RX is still needed to handle the ISI introduced by multipath propagation. Moreover, the signal processing associated with FDE, which includes fast Fourier transform (FFT), inverse fast Fourier transform (IFFT), and matrix inversion, can lead to a power hungry RX for giga-symbols-per-second systems. From the capacity perspective, on the other hand, Fig. 7 shows that the impact of the NLOS components is marginal and cannot notably improve the capacity of LOS GSM (see Section IV). These findings strongly motivate us to consider eliminating the NLOS components in the LOS scenario. Thanks to the specular nature of indoor propagation, the NLOS components can be avoided by using antennas with sufficient directivity or phased sub-arrays as shown in [20] for LOS SMX. This in turn helps to increase the antenna gain and improve the received SNR.

3) Multipath Channel with Un-Equalized Reception: In the previous paragraph, we have concluded that the NLOS components of the channel in the LOS scenario should be avoided. If the NLOS components are eliminated, ideally the channel becomes pure LOS and the received signal could be detected without the need of equalization. Motivated by this consideration, we study the potential of suppressing the NLOS components by discarding the measured CIR beyond a given maximum path length $dp_{\max}$ and study the SEP of GSM over the truncated measured channels. As mentioned, equalization is not needed in this case and, thus, we consider the low-complexity detection algorithm described in Appendix B-3. The simulation results are presented in Fig. 12. The SEP of GSM over the extracted LOS component of the measured channels is used as a benchmark.

Based on Fig. 5(a), we evaluate two case studies: $dp_{\max} = 4$ m and $dp_{\max} = 6$ m. As for $dp_{\max} = 6$ m, the SEP of GSM over the the truncated measured channels is significantly worse than that over the measured LOS component at moderate SNR (about 5 dB worse at an SEP level 10^{-2}). At high SNR, the SEP is limited by an error floor. The poor SEP performance is attributed to the reflected paths with path lengths in the range of $4.5 - 6$ m in Fig. 5(a). If we reduce $dp_{\max}$ to 4 m, which, in the considered setup, implies that all the major NLOS paths are eliminated, the SEP becomes reasonably good — within 2 dB in SNR as compared to that of the measured LOS component.

In conclusion, our experimental study shows that a simple RX without equalization may be a suitable low-complexity solution for LOS GSM communications, provided that the NLOS components are eliminated.
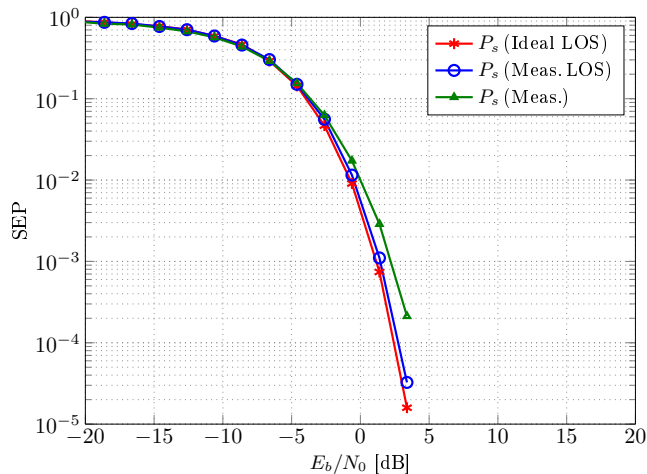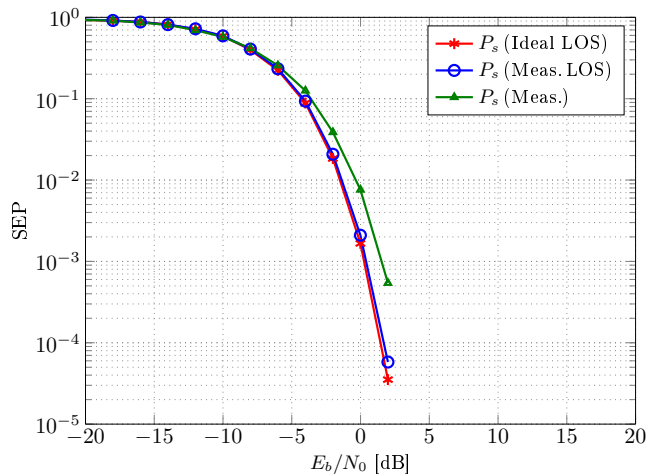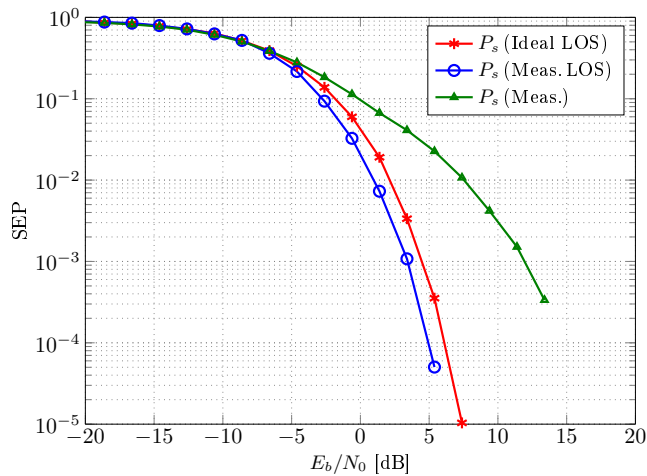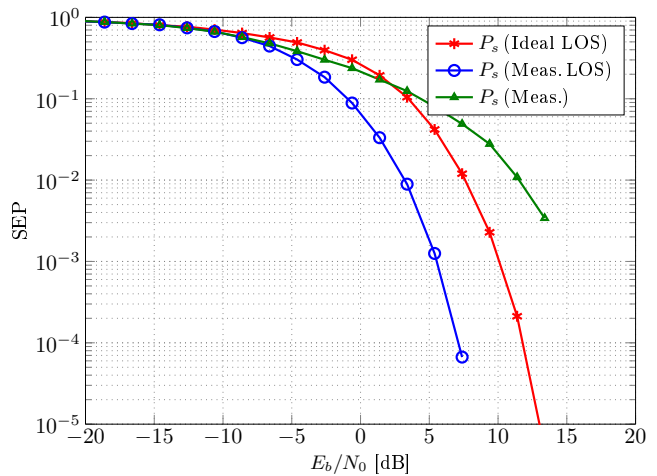
Fig. 10. Simulation results on the SEP of GSM over the measured channels (Scenario I). Legend: "Ideal LOS" — ideal pure LOS channels and using the ML detection algorithm as given in (7); "Meas. LOS" — LOS component extracted from the measured multipath channels and using (7); "Meas." — measured multipath channels including both LOS and NLOS components and using the SC-FDE algorithm as given in Appendix B-2.
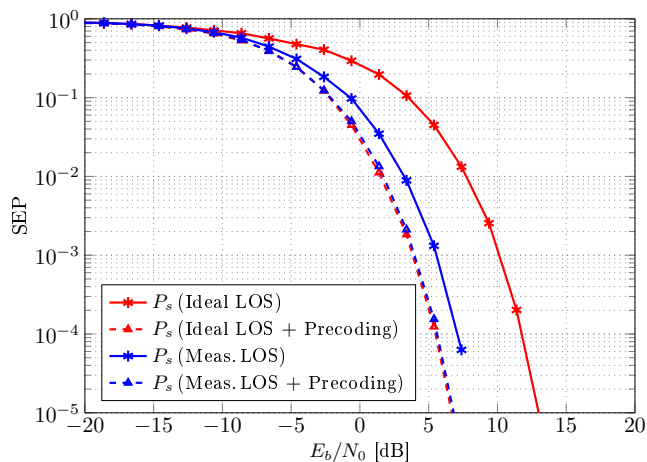

Fig. 11. Effect of precoding on the SEP of GSM. The setup and channel data are the same as Fig. 10(d). Legend: "Ideal LOS" — ideal pure LOS channels and using the ML detection algorithm as given in (7); "Meas. LOS" — LOS component extracted from the measured multipath channels and using (7); "Meas. LOS + Precoding" — Precoding is used on top of "Meas. LOS".

4) Impact of Richer Scattering and Close Reflections: As in Section IV-B3, we consider Scenario II and run the same set of simulations as the one used to generate Fig. 10 (a), (c) and (d). The representative results are illustrated in Fig. 13. The findings are as follows.

- As shown by the "Meas. LOS" curves in Fig. 13, close reflections destroy to some extent the channel orthogonality in the case of $\eta = 1$ thus degrading the GSM SEP (see Fig. 13 (a)). However, if the MIMO setup is largely under-separated, i.e., $\eta \gg 1$, the GSM SEP can be improved by the randomness introduced by close reflections (see Fig. 13 (b) for the case of $\eta = 4$).

- As shown by the "Meas." curves in Fig. 13, the NLOS components of the channel in the richer scattered environment produce results that lead to the same conclusions as those made for Scenario I in Section V-B2, i.e., NLOS components are generally harmful to the error performance of GSM because equalization would then be needed while the SEP can be even worse than the extracted LOS
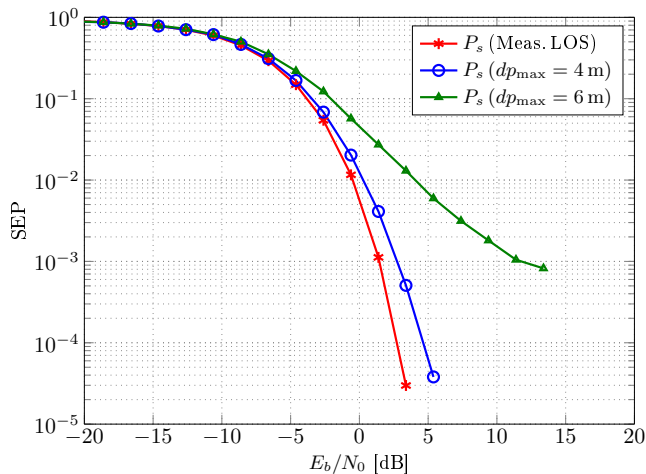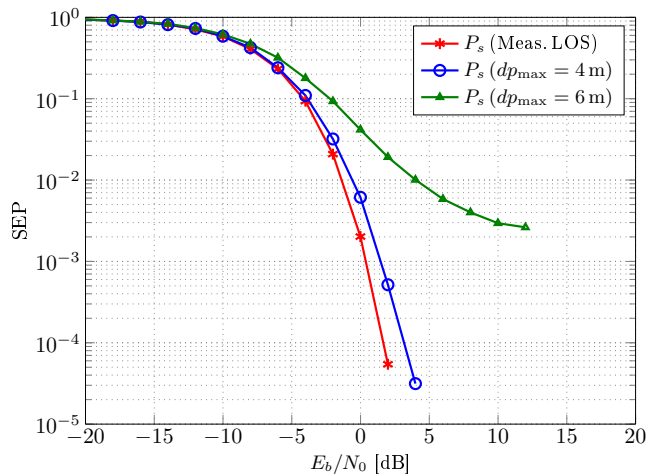
(a) Scenario I, $4 \times 4, \eta = 1$

(b) Scenario I, $6 \times 6, \eta = 1$

Fig. 12. Simulation results on the SEP of GSM over the measured channels (Scenario I). Legend: "Meas. LOS" — LOS component extracted from the measured multipath channels and using (7); $dp_{\max}$ — measured multipath channels and using the algorithm given in Appendix B-3, but the MIMO CIRs are truncated to include only paths with a path length not exceeding $dp_{\max}$.
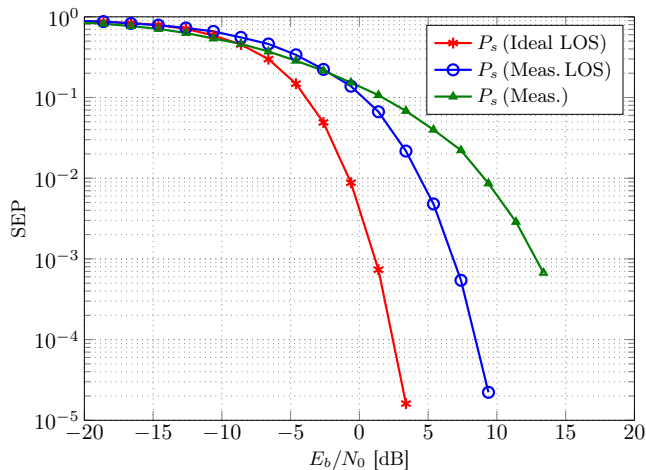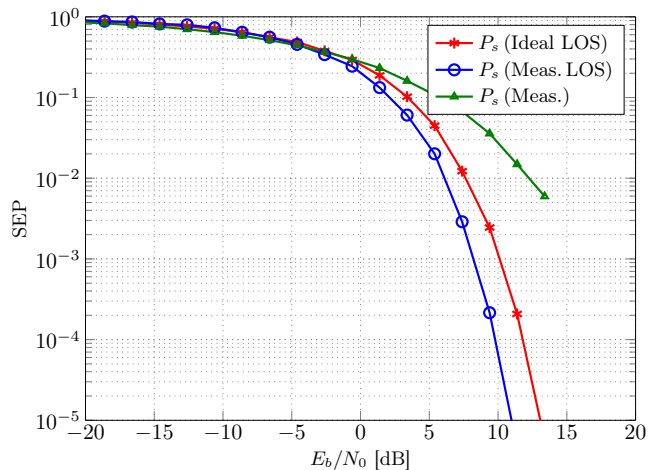

(a) Scenario II, 4×4 MIMO with $\eta = 1$

(b) Scenario II, 4×4 MIMO with $\eta = 4$

Fig. 13. Simulation results on the SEP of GSM (Scenario II). The legend terms are the same as in Fig. 10.

component.

VI. CONCLUSIONS

In this work, we performed channel sounding at 60 GHz in an indoor office environment and studied the capacity and SEP of GSM based on measured channel data. The major findings are as follows:

1) The capacity and SEP of GSM given in [14] based on ideal pure LOS analysis can indeed be achieved with the LOS component of the measured channels. The SEP of GSM in the LOS scenario can be minimized by properly separating the TX and RX antennas and making the MIMO channel orthogonal. Thus previous theoretical work in [14] is validated.

2) For capacity optimization, our results strongly suggest that precoding should be used with LOS GSM to simultaneously achive GSM capacity maximization and MIMO array size reduction. This finding is a necessary supplement to the SEP optimization of [14] and capacity optimization of [15].

3) The NLOS components of the measured channels, although can marginally improve the frequency-average capacity of GSM, are actually harmful for GSM in the presence of the LOS component. In communications with a symbol rate of the order of 1 GHz, the ISI introduced by the NLOS components spans tens of symbols. SC-FDE can handle this ISI but at the expenses of an increased hardware and signal processing complexity and a worse SEP as compared to the measured LOS component.

4) Despite of the cost and complexity introduced by the implementation of the equalizer, the SEP of SC-FDE GSM over multipath channels is worse than that over the measured LOS component and with direct detection. It is thus suggested to avoid the NLOS components in the

LOS scenario and design GSM communication systems that solely rely on LOS paths. As a result, a system with full simplicity (i.e., with both a simple TX and RX) can be used to achieve GSM communication, provided that the reflected paths are eliminated.

5) When the MIMO setup does not fulfill the orthogonality condition, i.e., $\eta \neq 1$, the SEP of GSM deteriorates over both the LOS component of the measured channels and the ideal pure LOS channels. However, the nonidealities in the measured LOS component showed potential to improve the SEP as compared to the ideal pure LOS channels. This suggests that channel randomness introduced by hardware nonidealities, close reflections and precoding can improve the SEP of GSM when the array antennas are largely not sufficiently separated (in regard to the orthogonal setup).

It has to be noted that the conclusion that the NLOS components are harmful and should be avoided is made based on using practical detectors. However, the capacity analysis shows that this may not be true if a capacity-achieving detector is used. This highlights that more complicated/optimal receivers may be needed in order to take advantage of the NLOS channels — even though the gain is expected not to be very significant. This research issue is left for further work.

APPENDIX A
CAPACITY EVALUATION ALGORITHMS

1) Frequency-Flat Channels: For capacity calculation, the system model given in (6) for LOS channels and discrete IQ symbols is extended into a more general form for any frequency-flat channels and a continuous-envelope IQ signal as

$$\mathbf{y} = \mathbf{H}\mathbf{e}_i s + \mathbf{n} = s \sum_{k \in \mathcal{I}_i} \mathbf{h}_k + \mathbf{n}, \tag{13}$$

where $\mathbf{H}$ is an $N_r \times N_t$ matrix of frequency-flat channel coefficients, $\mathbf{h}_k$ is the k-th column of $\mathbf{H}$, s is the (complex) IQ signal, and $\mathbf{e}_i$ and $\mathbf{n}$ are as defined in (6). According to [14, Theorem 1], the capacity achieved by GSM, using zero-mean complex Gaussian (ZMCG) signaling in the IQ domain and uniform signaling in the spatial domain, is given by (12) on page 14, where C_1 and C_2 are the IQ and spatial capacities respectively, $E_s \triangleq \mathbb{E}[|s|^2]$ is the average energy of the IQ symbol, $\mathbb{E}_{\mathbf{y}|i}[\cdot]$ is the expectation over the conditional random vector $\mathbf{y}$ (conditioned on i), $p(i)$ is the probability mass function (PMF) of i, $p(\mathbf{y}|i)$ is the conditional PDF of $\mathbf{y}$ given by

$$p(\mathbf{y}|i) = \frac{1}{|\pi \mathbf{\Gamma}_i|} \exp\left[-\mathbf{y}^{\mathrm{H}} \mathbf{\Gamma}_i^{-1} \mathbf{y}\right], \tag{14}$$

where $\mathbf{\Gamma}_i \in \mathbb{C}^{N_r \times N_r}$ is the co-variance matrix of $\mathbf{y}$ given by

$$\mathbf{\Gamma}_i = \frac{E_s}{N_u} \cdot \left[\sum_{k \in \mathcal{I}_i} \mathbf{h}_k\right] \left[\sum_{k \in \mathcal{I}_i} \mathbf{h}_k^{\mathrm{H}}\right] + N_0 \mathbf{I}, \tag{15}$$

where $\mathbf{H}$ and $\mathbf{h}_k$ are defined in (13), and $\gamma \triangleq E_s/N_0$ is the SNR. Note that we refer to the conceptual TX model shown in Fig. 1 and do not consider the power loss introduced by the

switch. As a result, E_s can be viewed as the average transmit power and γ can be interpreted as the average transmit power to noise power ratio.

2) Frequency-Selective Channels: In frequency-selective channels, the channel coefficients vary over frequencies. We calculate a frequency-average capacity of GSM as

$$C_{\mathrm{avg}} = \underbrace{\sum_{k=0}^{K} C_1\left(\mathbf{H}_f(k), \gamma\right)}_{C_{1,\mathrm{avg}}} + \underbrace{\sum_{k=0}^{K} C_2\left(\mathbf{H}_f(k), \gamma\right)}_{C_{2,\mathrm{avg}}}, \tag{16}$$

where $C_{1,\mathrm{avg}}$ and $C_{2,\mathrm{avg}}$ are the frequency-average IQ and spatial capacities respectively, $\mathbf{H}_f(k)$ given in (10) is the channel coefficients at the k-th frequency position. The above frequency-average capacity can be realized using an OFDM-style waveform, i.e., each sub-carrier is treated as an individual GSM channel with its own IQ stream and spatial modulation.

APPENDIX B
LINK-LEVEL SIMULATION

1) Transmission: For unified presentation of both algorithms, the link level transmission is assumed to be on a block basis: each K subsequent GSM symbols are regarded as a block, and a cyclic prefix (CP) of length at least $L - 1$, where L is the maximum number of channel taps, is added to each block at the TX. At the RX, the CP is first removed (before equalization or detection), thus the inter-block interference is avoided. The block of K GSM symbols, after being mapped to the TX antennas, can be expressed as

$$\mathbf{X} = \begin{bmatrix} x_1(1) & \cdots & x_1(K) \\ \vdots & \ddots & \vdots \\ x_{N_t}(1) & \cdots & x_{N_t}(K) \end{bmatrix} \in \mathbb{C}^{K \times N_t}, \tag{17}$$

where $x_i(k)$ denotes the transmitted signal on the i-th TX antenna within the k-th time slot. The block representation of the noise signal $\mathbf{N}$ and received signal $\mathbf{Y}$ are defined likewise. The transmission for one block, without explicitly showing the CP insertion and removal, can be expressed as

$$\underbrace{\begin{bmatrix} y_1(1) \\ \vdots \\ y_1(K) \\ \vdots \\ y_{N_r}(1) \\ \vdots \\ y_{N_r}(K) \end{bmatrix}}_{\triangleq \bar{\bar{\mathbf{y}}}} = \underbrace{\begin{bmatrix} \mathbb{H}_{11} & \cdots & \mathbb{H}_{1N_t} \\ \vdots & \ddots & \vdots \\ \mathbb{H}_{N_r 1} & \cdots & \mathbb{H}_{N_r N_t} \end{bmatrix}}_{\mathbb{H}} \underbrace{\begin{bmatrix} x_1(1) \\ \vdots \\ x_1(K) \\ \vdots \\ x_{N_t}(1) \\ \vdots \\ x_{N_t}(K) \end{bmatrix}}_{\triangleq \bar{\bar{\mathbf{x}}}} + \underbrace{\begin{bmatrix} n_1(1) \\ \vdots \\ n_1(K) \\ \vdots \\ n_{N_r}(1) \\ \vdots \\ n_{N_r}(K) \end{bmatrix}}_{\triangleq \bar{\bar{\mathbf{n}}}} \tag{18}$$

where $\bar{\bar{\mathbf{x}}}$, $\bar{\bar{\mathbf{n}}}$, and $\bar{\bar{\mathbf{y}}}$ are the transposed and stacked versions of the vectors $\mathbf{X}$, $\mathbf{N}$ and $\mathbf{Y}$ respectively, and $y_j(k)$ is the received signal on the j-th RX antenna within the k-th time slot. According to the noise definition in (6), we have $\mathbf{n} \sim \mathcal{CN}(\mathbf{0}, N_0 \mathbf{I}_{N_r K})$. The j, i-th sub-matrix of $\mathbb{H}$ is a circulant

$$C(\mathbf{H},\gamma) = \underbrace{\sum_i p(i) \left[\log_2 \left(1 + \frac{E_s}{N_u N_0} \left\| \sum_{k \in \mathcal{I}_i} \mathbf{h}_k \right\|^2 \right) \right]}_{C_1} + \underbrace{\log_2 \binom{N_t}{N_u} - \frac{1}{\binom{N_t}{N_u}} \sum_i \mathbb{E}_{\mathbf{y}|i} \left[\log_2 \frac{\sum_{i'} p(\mathbf{y}|i')}{p(\mathbf{y}|i)} \right]}_{C_2}, \quad (12)$$

matrix composed of the sampled version of the CIR $h_{ji}(\tau)$ in (2) (sampled at symbol rate) and is given by

$$\mathbb{H}_{ji} = \begin{bmatrix} h_{ji}(0) & h_{ji}(L-1) & \cdots & h_{ji}(1) \\ h_{ji}(1) & h_{ji}(0) & \cdots & h_{ji}(2) \\ \vdots & \vdots & \ddots & \vdots \\ h_{ji}(L-1) & h_{ji}(L-2) & \cdots & h_{ji}(0) \end{bmatrix}, \quad (19)$$

where $h_{ji}(k)$ is the k-th sample of $h_{ji}(\tau)$.

2) FDE Reception: The time-domain block transmission model given in (18) can be converted into the frequency domain using the discrete Fourier transform (DFT) as [36]

$$\underbrace{(\mathbf{I}_{N_r} \otimes \mathbf{U}) \cdot \bar{\bar{\mathbf{y}}}}_{\triangleq \bar{\bar{\mathbf{y}}}^f} = \mathbf{\Lambda} \cdot \underbrace{(\mathbf{I}_{N_r} \otimes \mathbf{U}) \cdot \bar{\bar{\mathbf{x}}}}_{\triangleq \bar{\bar{\mathbf{x}}}^f} + \underbrace{(\mathbf{I}_{N_r} \otimes \mathbf{U}) \cdot \bar{\bar{\mathbf{n}}}}_{\triangleq \bar{\bar{\mathbf{n}}}^f}, \quad (20)$$

where $\mathbf{U} = \mathbf{F}/\sqrt{K}$, with $\mathbf{F} = [\exp(-\mathrm{j}2\pi kl)]$ for $k, l = 0, 1, \ldots, K-1$, is the unitary DFT matrix, $\otimes$ is the Kronecker product operator, and

$$\mathbf{\Lambda} = \begin{bmatrix} \mathbf{\Lambda}_{11} & \cdots & \mathbf{\Lambda}_{1N_t} \\ \vdots & \ddots & \vdots \\ \mathbf{\Lambda}_{N_r 1} & \cdots & \mathbf{\Lambda}_{N_r N_t} \end{bmatrix} \quad (21)$$

with $\mathbf{\Lambda}_{ji}$ being a diagonal matrix of the frequency domain channel response between the i-th TX antenna and the j-th RX antenna given by

$$\mathbf{\Lambda}_{ji} = \mathrm{diag}\left(\mathbf{U}\mathbf{h}_{ji}\right). \quad (22)$$

It is important to note that, $\bar{\bar{\mathbf{x}}}^f$, $\bar{\bar{\mathbf{n}}}^f$, and $\bar{\bar{\mathbf{y}}}^f$ are the equivalent frequency-domain versions of $\bar{\bar{\mathbf{x}}}$, $\bar{\bar{\mathbf{n}}}$ respectively, and $\bar{\bar{\mathbf{y}}}$ and (20) is the equivalent frequency-domain model of the time-domain block-wise transmission system in (18). As a result, $\bar{\bar{\mathbf{x}}}^f$ can be recovered by frequency domain equalization as

$$\bar{\bar{\mathbf{x}}}_f^\dagger = \mathbf{W}\bar{\bar{\mathbf{y}}}_f \quad (23)$$

where $\mathbf{W}$ is the frequency-domain equalizer, and $\bar{\bar{\mathbf{x}}}_f^\dagger$ is the equalized frequency domain signal. For the considered SC-FDE receiver, the equalizer can be designed according to the zero forcing (ZF) or minimum mean square error (MMSE) criterion. It is well-known that the latter has superior performance, since it takes into account the noise power and eliminates the noise amplification issue. Furthermore, MMSE equalization has been commonly used in other SC-FDE systems for 60 GHz communications [37]–[39]. Hence, we also use MMSE equalization, which is given by [36]

$$\mathbf{W}_{\mathrm{MMSE}} = \frac{\mathbf{\Lambda}^{\mathrm{H}}}{N_t} \left(\frac{\mathbf{\Lambda}\mathbf{\Lambda}^{\mathrm{H}}}{N_t} + N_0 \mathbf{I}_{N_r K} \right)^{-1} \quad (24a)$$

$$= \left(\frac{\mathbf{\Lambda}^{\mathrm{H}}\mathbf{\Lambda}}{N_t} + N_0 \mathbf{I}_{N_t K} \right)^{-1} \frac{\mathbf{\Lambda}^{\mathrm{H}}}{N_t}, \quad (24b)$$

where (24b) is known as the alternative form of the MMSE equalizer which is obtained by applying the matrix inversion lemma [40, (9)] to (24a). The alternative form is more computationally efficient than the original form for $N_r > N_t$.

Once the received signal is equalized, it is converted back into the time domain as

$$\bar{\bar{\mathbf{x}}}^\dagger = \left(\mathbf{I}_{N_t} \otimes \mathbf{U}^{\mathrm{H}}\right) \bar{\bar{\mathbf{x}}}_f^\dagger. \quad (25)$$

Finally, we use ML detection to recover the GSM symbols as

$$\hat{\mathbf{x}}(k) = \arg\min_{\mathbf{x} \in \mathbb{S}} \left\| \mathbf{x}^\dagger(k) - \mathbf{x} \right\|^2 \quad \forall k = 1, 2, \ldots, K, \quad (26)$$

where $\mathbf{x}^\dagger(k) \triangleq \left[x_1^\dagger(k), x_2^\dagger(k), \ldots, x_{N_t}^\dagger(k) \right]^T$ is the un-stacked version of $\bar{\bar{\mathbf{x}}}^\dagger$, the mapping of $x_i^\dagger(k)$ in $\bar{\bar{\mathbf{x}}}^\dagger$ is similar to the mapping of $x_i(k)$ in $\bar{\bar{\mathbf{x}}}$ in (18). For the whole block, we have $\widehat{\mathbf{X}} = [\hat{\mathbf{x}}(1), \hat{\mathbf{x}}(2), \ldots, \hat{\mathbf{x}}(K)]$. If no error occurs, we have $\widehat{\mathbf{X}} = \mathbf{X}$. The simulated SEP is calculated as the ratio of the number of wrongly detected GSM symbols to the total number of GSM symbols sent.

3) Un-Equalized Reception: In the non-equalized reception, following (18), the received signal is directly detected without conversion into the frequency domain. The ML detection in this case is written as

$$\hat{\mathbf{x}}(k) = \arg\min_{\mathbf{x} \in \mathbb{S}} \left\| \mathbf{y}(k) - \mathbf{H}_{\mathrm{LOS}}\mathbf{x} \right\|^2 \quad \forall k = 1, 2, \ldots, K, \quad (27)$$

where $\mathbf{H}_{\mathrm{LOS}}$ is the LOS component of the measured channel, $\mathbf{y}(k) = [y_1(k), y_2(k), \ldots, y_{N_r}(k)]^T$ is the received signal given in (18). The simulated SEP is calculated similarly as above in the previous case.

REFERENCES

[1] M. Di Renzo, H. Haas, A. Ghrayeb, S. Sugiura, and L. Hanzo, "Spatial modulation for generalized MIMO: Challenges, opportunities, and implementation," *Proc. IEEE*, vol. 102, no. 1, pp. 56–103, Jan. 2014.

[2] A. Younis, W. Thompson, M. Di Renzo, C.-X. Wang, M. Beach, H. Haas, and P. Grant, "Performance of spatial modulation using measured real-world channels," in *2013 IEEE 78th Veh. Technol. Conf. (VTC Fall)*, Sep. 2013, pp. 1–5.

[3] N. Serafimovski, A. Younis, R. Mesleh, P. Chambers, M. Di Renzo, C.-X. Wang, P. Grant, M. Beach, and H. Haas, "Practical implementation of spatial modulation," *IEEE Trans. Veh. Technol.*, vol. 62, no. 9, pp. 4511–4523, Nov. 2013.

[4] J. Zhang, Y. Wang, L. Ding, and N. Zhang, "Bit error probability of spatial modulation over measured indoor channels," *IEEE Trans. Wireless Commun.*, vol. 13, no. 3, pp. 1380–1387, Mar. 2014.

[5] K. M. Humadi, A. I. Sulyman, and A. Alsanie, "Experimental results for generalized spatial modulation scheme with variable active transmit antennas," in *Cognitive Radio Oriented Wireless Networks*, ser. Lecture Notes of the Inst. for Comput. Sci., Social Informatics and Telecommun. Eng. Springer Int. Publishing, Apr. 2015, no. 156, pp. 260–270.

[6] G. J. Foschini, "Layered space-time architecture for wireless communication in a fading environment when using multi-element antennas," *Bell Labs Tech. J.*, vol. 1, no. 2, pp. 41–59, 1996.

[7] P. Wolniansky, G. Foschini, G. Golden, and R. Valenzuela, "V-BLAST: An architecture for realizing very high data rates over the rich-scattering wireless channel," in *URSI Int. Symp. on Signals, Systems, and Electronics*, Sep. 1998, pp. 295–300.

[8] J. Wang, S. Jia, and J. Song, "Generalised spatial modulation system with multiple active transmit antennas and low complexity detection scheme," *IEEE Trans. Wireless Commun.*, vol. 11, no. 4, pp. 1605–1615, Apr. 2012.

[9] A. Younis, "Spatial modulation: Theory to practice," Ph.D. dissertation, University of Edinburgh, 2014. [Online]. Available: http://hdl.handle.net/1842/8990

[10] O. Osman, "Variable active antenna spatial modulation," *IET Microwaves, Antennas & Propagation*, vol. 9, no. 15, pp. 1816–1824, dec 2015.

[11] A. Stavridis, S. Sinanovic, M. Di Renzo, and H. Haas, "Energy evaluation of spatial modulation at a multi-antenna base station," in *IEEE 78th Veh. Technol. Conf. (VTC Fall)*, Sep. 2013, pp. 1–5.

[12] P. Patcharamaneepakorn, S. Wu, C. X. Wang, e. H. M. Aggoune, M. M. Alwakeel, X. Ge, and M. D. Renzo, "Spectral, energy, and economic efficiency of 5G multicell massive MIMO systems with generalized spatial modulation," *IEEE Trans. Veh. Technol.*, vol. 65, no. 12, pp. 9715–9731, Dec. 2016.

[13] P. Liu and A. Springer, "Space shift keying for LOS communication at mmWave frequencies," *IEEE Wireless Commun. Lett.*, vol. 4, no. 2, pp. 121–124, Apr. 2015.

[14] P. Liu, M. Renzo, and A. Springer, "Line-of-sight spatial modulation for indoor mmWave communication at 60 GHz," *IEEE Trans. Wireless Commun.*, vol. 15, no. 11, pp. 7373–7389, Nov. 2016.

[15] P. Liu, M. Di Renzo, and A. Springer, "Variable-N_u generalized spatial modulation for indoor LOS mmwave communication: Performance optimization and novel switching structure," *IEEE Trans. on Commun.*, vol. PP, no. 99, pp. 1–16, 2017.

[16] N. Ishikawa, R. Rajashekar, S. Sugiura, and L. Hanzo, "Generalized spatial modulation based reduced-RF-chain millimeter-wave communications," *IEEE Trans. Veh. Technol.*, vol. PP, no. 99, pp. 1–1, 2016.

[17] N. S. Perović, P. Liu, M. D. Renzo, and A. Springer, "Receive spatial modulation for LOS mmWave communications based on TX beamforming," *IEEE Commun. Lett.*, vol. 21, no. 4, pp. 921–924, Apr. 2017.

[18] A. Maltsev, V. Erceg, E. Perahia, C. Hansen, R. Maslennikov, A. Lomayev, A. Sevastyanov, A. Khoryaev, G. Morozov, M. Jacob, S. Priebe, T. Kürner, S. Kato, H. Sawada, K. Sato, and H. Harada, "Channel models for 60 GHz WLAN systems," Tech. Rep. IEEE 802.11-09/0334r8, May 2010. [Online]. Available: https://mentor.ieee.org/802.11/dcn/09/11-09-0334-08-00ad-channel-models-for-60-ghz-wlan-systems.doc

[19] F. Bohagen, P. Orten, and G. Oien, "Design of optimal high-rank line-of-sight MIMO channels," *IEEE Trans. Wireless Commun.*, vol. 6, no. 4, pp. 1420–1425, Apr. 2007.

[20] E. Torkildson, U. Madhow, and M. Rodwell, "Indoor millimeter wave MIMO: Feasibility and performance," *IEEE Trans. Wireless Commun.*, vol. 10, no. 12, pp. 4150–4160, Dec. 2011.

[21] William C. Jakes, "Multipath interference," in *Microwave Mobile Communications*. IEEE Press, 1974.

[22] H. Friis, "A note on a simple transmission formula," *Proc. IRE*, vol. 34, no. 5, pp. 254–256, May 1946.

[23] K. Sato, H. Kozima, H. Masuzawa, T. Manabe, T. Ihara, Y. Kasashima, and K. Yamaki, "Measurements of reflection characteristics and refractive indices of interior construction materials in millimeter-wave bands," in *IEEE 45th Veh. Tech. Conf.*, vol. 1, Jul. 1995, pp. 449–453 vol.1.

[24] J. Jeganathan, A. Ghrayeb, and L. Szczecinski, "Spatial modulation: Optimal detection and performance analysis," *IEEE Commun. Lett.*, vol. 12, no. 8, pp. 545–547, Aug. 2008.

[25] F. Bohagen, P. Orten, and G. E. Oien, "Construction and capacity analysis of high-rank line-of-sight MIMO channels," in *IEEE Wireless Commun. and Networking Conf.*, vol. 1, 2005, pp. 432–437.

[26] A. Chandra, A. Prokeš, T. Mikulášek, J. Blumenstein, P. Kukolev, T. Zemen, and C. F. Mecklenbräuker, "Frequency-domain in-vehicle UWB channel modeling," *IEEE Trans. Veh. Technol.*, vol. 65, no. 6, pp. 3929–3940, JUNE 2016.

[27] J. Blumenstein, A. Prokes, A. Chandra, T. Mikulasek, R. Marsalek, T. Zemen, and C. Mecklenbräuker, "In-vehicle channel measurement, characterization and spatial consistency comparison of 3-11 GHz and 55-65 GHz frequency bands," *IEEE Trans. Veh. Technol.*, vol. PP, no. 99, 2016.

[28] J. Blumenstein, J. Vychodil, M. Pospisil, T. Mikulasek, and A. Prokes, "Effects of vehicle vibrations on mm-wave channel: Doppler spread and correlative channel sounding," in *IEEE 27th Annual Int. Symp. on Personal, Indoor, and Mobile Radio Commu. (PIMRC)*, Sep. 2016, pp. 432–437.

[29] H. Xu, V. Kukshya, and T. Rappaport, "Spatial and temporal characteristics of 60-GHz indoor channels," *IEEE J. Sel. Areas Commun.*, vol. 20, no. 3, pp. 620–630, Apr. 2002.

[30] T. Pedersen, G. Steinbock, and B. Fleury, "Modeling of reverberant radio channels using propagation graphs," *IEEE Trans. Antennas Propag.*, vol. 60, no. 12, pp. 5978–5988, Dec 2012.

[31] N. S. Perović, P. Liu, and A. Springer, "Design of a simple phase precoder for generalized spatial modulation in los millimeter wave channels," in *11th int. ITG conf. on systems communications and coding (SCC17)*, 2017.

[32] C. Masouros and L. Hanzo, "Constellation randomization achieves transmit diversity for single-RF spatial modulation," *IEEE Trans. Veh. Technol.*, vol. 65, no. 10, pp. 8101–8111, Oct. 2016.

[33] P. Yang, Y. Xiao, Y. L. Guan, K. V. S. Hari, A. Chockalingam, S. Sugiura, H. Haas, M. Di Renzo, C. Masouros, Z. Liu, L. Xiao, S. Li, and L. Hanzo, "Single-carrier SM-MIMO: A promising design for broadband large-scale antenna systems," *IEEE Commun. Surveys Tuts.*, vol. 18, no. 3, pp. 1687–1716, 2016.

[34] R. W. Heath, "Millimeter wave MIMO: A signal processing perspective," Apr. 2015. [Online]. Available: http://users.ece.utexas.edu/rheath/presentations/2015/MmWaveMIMOaSPPerspectiveICASSP2015Heath.pdf

[35] O. E. Ayach, S. Rajagopal, S. Abu-Surra, Z. Pi, and R. W. Heath, "Spatially sparse precoding in millimeter wave MIMO systems," *IEEE Trans. Wireless Commun.*, vol. 13, no. 3, pp. 1499–1513, Mar. 2014.

[36] S. Sugiura and L. Hanzo, "Single-RF spatial modulation requires single-carrier transmission: Frequency-domain turbo equalization for dispersive channels," *IEEE Trans. Veh. Technol.*, vol. PP, no. 99, pp. 1–1, 2014.

[37] C. Park and T. S. Rappaport, "Short-range wireless communications for next-generation networks: UWB, 60 GHz millimeter-wave WPAN, and ZigBee," *IEEE Wireless Commun.*, vol. 14, no. 4, pp. 70–78, 2007.

[38] M. Lei, I. Lakkis, H. Harada, and S. Kato, "MMSE-FDE based on estimated SNR for single-carrier block transmission (SCBT) in multi-Gbps WPAN (IEEE 802.15.3c)," in *IEEE Int. Conf. on Commu. Workshops*, May 2008, pp. 52–56.

[39] F. Hsiao, A. Tang, D. Yang, M. Pham, and M.-C. F. Chang, "A 7Gb/s SC-FDE/OFDM MMSE equalizer for 60GHz wireless communications," in *IEEE Asian Solid State Circuits Conf.*, 2011, pp. 293–296.

[40] L. Szczecinski and D. Massicotte, "Low complexity adaptation of MIMO MMSE receivers, implementation aspects," in *IEEE Global Telecommun. Conf. (GLOBECOM)*, vol. 4, Dec. 2005, pp. 2327–2332.